Food Research International 229 (2026) 118520

Contents lists available at ScienceDirect

Food Research International

journal homepage: www.elsevier.com/locate/foodres

Synergistic curdlan gum/xanthan gum system improves shrimp myofibrillar protein gel properties via enhanced network structure, texture and water holding capacity

Shuling Zhou, Xuening Yu, Menghan Wang, Xiaoyang Liu *, Dayong Zhou

SKL of Marine Food Processing & Safety Control, National Engineering Research Center of Seafood, Collaborative Innovation Center of Seafood Deep Processing, Liaoning Province Key Laboratory for Marine Food Science and Technology, School of Food Science and Technology, Dalian Polytechnic University, Dalian 116034, China

ARTICLE INFO

Keywords:
Curdlan gum
Xanthan gum
Shrimp myofibrillar protein
Gel property
Texture
Water distribution

ABSTRACT

This study investigated the impact of varying curdlan gum (CG)/xanthan gum (XG) ratios (10:0, 7:3, 5:5, 3:7, 0:10) on the properties of shrimp myofibrillar protein (MP) gels. A CG:XG ratio of 5:5 significantly enhanced gel texture and water holding capacity, yielding maximum hardness (99 g higher than control) and the strongest gel network while this optimal ratio also promoted water immobilization, shifting free water to more fixed states. FTIR indicated hydrogen bond formation between CG-XG and MPs, facilitated by their helical structures. Rheology confirmed viscoelastic solid behavior, with elevated storage (G') and loss (G") moduli peaking at 5:5. CG-XG addition improved thermal stability while microstructural analysis (AFM, Cryo-SEM) revealed the 5:5 gel possessed the densest, most uniform network with minimal voids. Overall, CG-XG (5:5) showed effective enhancement of MP gel quality, providing a theoretical foundation for their rational use in shrimp products and innovative applications of compound polysaccharides.

1. Introduction

Myofibrillar protein (MP) is a crucial protein that constitutes myofibrils in muscle, accounting for approximately 50% to 55% of the total protein content in muscle. It is crucial in determining the final quality of processed meats (Gong et al., 2022). Due to its ability to form a three-dimensional gel network structure through a heat induction process, MPs significantly affects the functional characteristics of meat products (Jiang et al., 2025). Moreover, water holding capacity (WHC) is a vital functional property of MP gels, determining how much water remains bound in the gel network, consequently, these factors determine the quality of the finished product. However, the unique functional attributes exhibited by MPs, such as their emulsifying and gelling properties, are influenced by various factors, including the quality of raw meat, pH value, and ionic strength (Feng et al., 2023). Therefore, from a practical perspective, the addition of various natural polymers (such as non-meat proteins, food gels, and soluble dietary fibers) appears to be a more straightforward and effective approach to enhance the functional properties of myofibrillar proteins, ultimately leading to higher quality meat products. Among these natural polymers, certain food gels, particularly carrageenan and xanthan gel, have been shown to significantly improve the functional properties of MPs and are widely utilized in the production of related meat products (Zhang, Bai, et al., 2025).

Recent scientific investigations have demonstrated that polysaccharides are increasingly utilized as multifunctional ingredients in reduced-fat meat formulations. Serving as effective fat replacers, binding agents, and bulking compounds, these carbohydrate polymers significantly improve textural properties, water-holding capacity, and product acceptability. Furthermore, nutritional analyses confirm that polysaccharide not only boosts the dietary fiber content but also enhances the nutritional profile of meat products, addressing modern consumer demands for healthier food options (Wang et al., 2023). The molecular structure of polysaccharides is characterized by the presence of numerous hydrophilic groups, which interact with MPs through non-covalent interactions. These interactions, including hydrogen bonding, electrostatic interactions, and hydrophobic interactions, enhance the three-dimensional network structure, thereby improving the gelling characteristics of meat products. Influences of three polysaccharides on MPs gels properties by analyzing MPs gels phase behavior and moisture stability are reported while the polysaccharides have a strong ability to retain water, reduced the leakage of water from the gel network and

* Corresponding author.
E-mail address: liuxiaoyang0213@126.com (X. Liu).

https://doi.org/10.1016/j.foodres.2026.118520
Received 19 September 2025; Received in revised form 23 December 2025; Accepted 25 January 2026
Available online 26 January 2026
0963-9969/© 2026 Elsevier Ltd. All rights are reserved, including those for text and data mining, AI training, and similar technologies.

hindered the integrity of the MPs gels network (Zhuang et al., 2020). Hui et al. have demonstrated that adding blackberry polysaccharides to chicken breast meat is conducive to the diffusion of MPs protein structures. This not only enhances the hydrogen bonds and disulfide bonds of MPs molecules but also strengthens their network structure, thereby improving the final performance of the meat products (Teng et al., 2023).

Xanthan gum (XG) is an extracellular acidic polysaccharide characterized by low concentration and high viscosity. It exhibits an effective thickening capability, which mitigates the incompatibility between the oil and water phases, thereby enhancing the emulsification and stability of food systems. XG solutions demonstrate exceptional suspensibility, pseudoplasticity, and safety, significantly improving the eating quality of meat products, including attributes such as water holding capacity and tenderness (Souza & Garcia-Rojas, 2017). Concurrently, the incorporation of various food gels with unique functional characteristics into meat products has emerged as a prominent area of research. Curdlan gum (CG), a linear macromolecule formed by glucose through (1–3)-β-glycosidic links, possesses notable gelation, water retention, and thickening properties, along with good compatibility with hydrophobic substances. Its suspension exhibits the ability to form both hard, elastic thermal irreversible gels and thermal reversible gels upon heating (Hou et al., 2024). Previous studies have indicated that the addition of CG to meat products effectively reduces cooking loss, enhances emulsion stability, and significantly improves the sensory quality of the products (Ganie et al., 2024). In actual meat processing, the combination of different types of food gels can produce synergistic effects, improve the texture, flavor, and overall taste of meat products, while also offer advantages such as ease of use, simplicity of the process, and cost-effectiveness.

Although both CG and XG exhibit potential in enhancing the quality of meat products, the mechanisms underlying their combined application remain unclear. Notably, CG and XG differ significantly in molecular conformation and gel behavior: CG tends to form a rigid, thermally irreversible three-dimensional network, whereas XG primarily contributes a highly viscoelastic and flexible thickening effect, suggesting the possibility of functional complementarity between the two. We hypothesize that through appropriate proportioning, the rigid framework of CG and the flexible segments of XG may interact, potentially leading to the formation of an interpenetrating 'rigid-flexible' composite network structure during the thermal gelation of myofibrillar protein. This interaction may collaboratively enhance gel texture, water retention, and stability. However, there is currently a lack of systematic research on the action mechanisms and microscopic interactions of CG and XG in shrimp meat protein gels. Therefore, this study aims to systematically evaluate the effects of varying quality ratios of CG and XG on the gel properties of shrimp myofibrillar protein by regulating these ratios.

In this study, composite gels ingredients, specifically CG and XG, were combined in designated ratios (10:0, 7:3, 5:5, 3:7, 0:10, w/w) and added to shrimp muscle fiber protein at a 2% concentration before being subjected to heating to form a gel. The effects of these food composite gels on the emulsification, gel properties, and microstructure of MPs were systematically investigated. In order to clarify the structure-function relationship of polysaccharide-modified shrimp MPs gel, a variety of characterization methods were adopted, such as X-ray diffraction (XRD) for crystal domain analysis, Fourier-transform infrared spectroscopy (FTIR) for functional group determination, and scanning electron microscopy (SEM) for morphology detection. It is used to analyze how different polysaccharide ratios affect the structure and morphology of shrimp MPs gels. Additionally, differential scanning calorimetry (DSC) and water holding capacity (WHC) assessments were conducted to evaluate the properties of the MPs gels. To further explore the impact of polysaccharide ratios on MPs gels, the effects of polysaccharide treatment on moisture distribution, rheological properties, and microstructure of the MPs gels were examined using low-field nuclear magnetic resonance (NMR), rheology, atomic force microscopy (AFM), and cold field emission scanning electron microscopy (Cryo-SEM). This study underscores the potential application value of composite gels, providing a theoretical foundation and practical guidance for their rational use in shrimp products and paving the way for innovative applications of compound polysaccharides in the food industry.

2. Materials and methods

2.1. Materials and reagents

Shrimp (*Penaeus vannamei*) was purchased from local market in Dalian, China. Curdlan gum was purchased from Jiangsu Yiming Biological Co., Ltd. (Jiangsu, China). Xanthan gel was sourced from Xinjiang Plum Blossom Amino Acid Co., Ltd. (Xinjiang, China). Analytical-grade NaCl, $MgCl_2$, K_2HPO_4, and KH_2PO_4, as well as ethylenediaminetetraacetic acid (EDTA), were procured from Tianjin Damao Chemical Reagent Factory. (Tianjin, China).

2.2. Extraction and preparation of MP

Make slight modifications on the basis of the previous methods (Li, Li, et al., 2024), 200 g of shrimp meat was homogenized in 800 mL of extraction buffer, the extraction buffer (800 mL, pH 7.0) was prepared using 0.1 M NaCl, 1 mM EDTA, 2 mM $MgCl_2$, and 0.1 M Na_2HPO_4/NaH_2PO_4. Subsequently, 200 g of shrimp meat was homogenized twice (10,000 rpm, 2 min) in the extraction buffer, followed by centrifugation at 7990 rpm for 10 min. The residue was washed twice under identical conditions with 800 mL of 0.1 M NaCl solution. Finally, the collected residue was stored at 4 °C and utilized within 48 h. Protein concentration was determined using the Coomassie Brilliant Blue method, with bovine serum albumin (BSA) as the standard.

2.3. Preparation of MPs-CG-XG mixture

The experimental method was slightly modified based on the research (Li et al., 2021). The concentration of MPs was adjusted to 45 mg/mL using a buffer solution composed of 20 mM sodium phosphate and 0.6 M NaCl at pH 6.5. Subsequently, 2 g of MPs was transferred into tubes and mixed with 2% of CG-XG mixture in various ratios of 10:0, 7:3, 5:5, 3:7, and 0:10 (w/w). The mixture was stirred thoroughly and stored at 4 °C for future use.

2.4. Particle size distribution and zeta potential measurements

The MPs-CG-XG mixture prepared in section 2.3 was diluted to a concentration of 1 mg/mL using distilled water. Static laser particle analysis (DT-1202, Dispersion Technology Inc., New York, USA) was conducted to measure the Zeta potential and particle size distribution of the samples, with each measurement performed in triplicate.

2.5. Fluorescence spectrum

The MPs-CG-XG mixture prepared in Section 2.3 was diluted to a final concentration of 2 mg/mL using distilled water. Fluorescence emission spectra were acquired using a fluorescence spectrophotometer (HitachiF-2700, Hitachi Ltd., Tokyo, Japan) with an excitation wavelength of 280 nm and an emission wavelength scanning range of 300–420 nm. Both excitation and emission slit widths were set at 5.0 nm.

2.6. UV–vis absorption spectroscopy

The concentration of the MPs-CG-XG mixture, prepared as described in section 2.3, was adjusted to 1 mg/mL using distilled water. Spectra were recorded with a UV-1800 spectrophotometer (Lambda 35,

PerkinElmer, Waltham, Massachusetts, USA), scanning within the wavelength range of 190 to 450 nm.

2.7. Preparation of MPs-CG-XG gels

Composite hydrogels were formulated at a constant total biopolymer concentration of 2% (w/w) with varying mass ratios of CG to XG (10:0, 7:3, 5:5, 3:7, and 0:10). Precisely weighed quantities of CG and XG powders were thoroughly blended with 10 g of MPs. The mixtures were homogenized by vigorous stirring, subsequently incubated in a temperature-controlled water bath at 45 °C for 15 min, and then subjected to microwave irradiation (140 W, 10 s). The gels were refrigerated at 4 °C overnight prior to subsequent testing.

2.8. Texture profile analysis (TPA)

The Texture Profile Analyzer (TA.XT. plus, Stabilized Microsystems, Surrey, UK) was employed for the texture characterization. Elliptical samples, measuring 10 mm in height and 20 mm in diameter, were prepared and analyzed using a cylindrical probe (P/50). The test parameters were established as follows: a pre-test speed of 2 mm/s, a test speed of 1 mm/s, a return speed of 2 mm/s, a target mode set to strain, a target value of 40%, a trigger force of 5 g, and an interval time of 5 s. Each group of samples was measured 5 to 6 times, and the average value was recorded.

2.9. Color properties analysis

The color changes of MPs-CG-XG gel samples were determined using a colorimeter (Ultra Scan Pro, Hunter Lab, Fairfax, Virginia, USA). Calibrate use standard whiteboards and standard blackboards. The sample was placed over the measurement port, and the measurement was conducted in reflectance mode. Among them, L* represents the brightness, and a*(+a represents red; −a represents green), b* (+b represents yellow; −b represents blue). The experiment was conducted three times.

2.10. Gel strength

The mechanical strength of the gels was determined using a TA texture analyzer (TA.XT. plus, Stabilized Microsystems, Surrey, UK) equipped with a P/0.5 cylindrical probe. The testing parameters were set as follows: pre-test and post-test speed of 5 mm/s, test speed of 1 mm/s, penetration depth of 15 mm, and trigger force of 3 g. Gel strength was calculated as the product of breaking force and corresponding indentation depth at the point of rupture Gel strength = fracture strength×depression depth.

2.11. WHC

The determination of WHC in the gels of MPs-CG-XG necessitated centrifugation at 5000 rpm for 20 min at a temperature of 4 °C. The formula for calculating water retention was outlined as follows:

$$\text{WHC}\ (\%) = [(M - (M_1 - M_2)/M] \times 100$$

where M represents the total mass of gels (g), M_1 represents the total mass of absorbent paper after centrifugation (g), and M_2 represents the mass of absorbent paper before centrifugation (g). Each group was tested three times and the average value was taken.

2.12. Lf-NMR

To evaluate the distribution of water in MPs-CG-XG gels, we conducted low-frequency nuclear magnetic resonance (LF-NMR) analysis using nuclear magnetic resonance (MRI) analyzer (MesoQMR23-060H, Shanghai Niu Mai, Shanghai, China). Approximately 10 g of gel sample was placed into an NMR tube for signal acquisition. The pulse parameters typically recorded include a spectrometer frequency (SF) of 21 MHz, a spectrometer width (SW) of 200 kHz, a number of scans (NS) of 4, test latency (TW) of 1500 ms, echo time (TE) of 0.5 ms, and a number of echoes (NECH) of 12,000. The measured value of the transverse relaxation time T_2 was obtained through software inversion.

2.13. MRI assay

The MRI was used to investigate the water distribution while T_2-weighted images of the MPs-CG-XG gels were acquired using spin echo (SE) sequences with the following parameters: slice thickness of 3 mm, a mean of 2, echo time of 20 ms, and a repetition time of 2100 ms. The analysis of the T_2-weighted images was conducted using specialized software (OsiriX Life v.7.0.4, Pximeo, Geneva, Switzerland).

2.14. FTIR

FTIR spectral (Spectrum Two, PerkinElmer, Waltham, Massachusetts, USA) analysis was conducted on the freeze-dried MPs-CG-XG composite gel. The sample was uniformly mixed with potassium bromide (KBr) at a ratio of 1:100 and finely ground using an agate mortar. The obtained powder is compressed into suitable transparent discs. The resolution is 4 cm^{-1} and the test range is 4000 to 400 cm^{-1}. Before sample analysis, background correction was performed using pure KBr particles.

2.15. XRD

The X-ray diffraction patterns of MPs-CG-XG gels were tested using an XRD diffractometer (XRD-7000S, Shimadzu, Kyoto, Japan) with the following parameter range of 10–80° 2θ and a scanning rate of 5°/min. The freeze-dried gel samples were evenly placed in the sample holder for analysis.

2.16. Rheological test

The rheological properties of the MPs-CG-XG gels were evaluated using a Discovery rheometer (TA-DHR 2, TA Instrument, New Castle, UK) equipped with parallel plates (40 mm). Oscillatory strain sweep: The strain sweep range was 0.1%–100% when a frequency of 1.0 Hz was determined. Frequency Sweep Analysis: A frequency sweep was performed from 0.1 to 10 Hz while the stress was maintained at a constant strain of 1.0% in the linear viscoelastic region. Steady state shear measurement: For steady state testing, the sample was sheared continuously at rates from 0.1 to 100 s^{-1} to measure apparent viscosity (η). Dynamic frequency sweeps (0.1–10 Hz, 1.0% strain) assessed viscoelastic properties within the LVR. Steady shear rheology (0.1–100 s^{-1}) evaluated shear-thinning behavior through apparent viscosity (η) measurements.

2.17. DSC and TGA

The thermal properties of the MPs-CG-XG gels were investigated using thermogravimetry and differential scanning calorimetry (STA 449 F5, Netzsch, Selb, Germany). About 5 mg of sample was placed in a crucible and heated from 20 °C to 500 °C at a rate of 10 °C/min in a nitrogen atmosphere. The endothermic peaks and related transition temperatures during heating were recorded and analyzed.

2.18. AFM

AFM imaging was performed using a Hitachi AFM (AFM5500, Hitachi Ltd., Tokyo, Japan). MPs-CG-XG gels was diluted to 1 μg/mL with distilled water, deposited on freshly cut mica sheets, dried, and then imaged at room temperature at a scan rate of 0.2 Hz over a scan

area of 10 × 10 μm. AFM 5000 II software was used to analyze and estimate molecular heights.

2.19. SEM

The microstructure of MPs-CG-XG gel samples was observed using a SEM (JSM-7800F, Jeol, Tokyo, Japan) in accordance with the following methods. The prepared gel samples were freeze-dried for 48 h. The samples were placed on the SEM carrier stage and gold was sprayed for 50 × observation.

2.20. Cryo-SEM

The microstructure of MPs-CG-XG gels samples was observed by Cryo-SEM (SU8010, Hitachi Ltd., Tokyo, Japan). During this process, the samples were rapidly frozen in liquid nitrogen slurry, then sprayed with gold and cooled again, and the differences in microstructure were observed at 2000 × and 5000 × magnifications, respectively.

2.21. Statistical analysis

All characterizations were performed at least three times using randomly selected samples, and the data are reported as means ± SD. Statistical analyses were conducted using SPSS (Version 19.0, IBM Co., Ltd., New York, USA), employing one-way ANOVA with Duncan's post hoc testing and Student's *t*-tests for pairwise comparisons. Statistical significance was defined as $P < 0.05$ for all analyses. The result graphs in this study were generated using Origin 2021 software (OriginLab Co., Ltd., MA, USA).

3. Results and discussion

3.1. Characterizations of MPs-CG-XG mixture in different ratios

In order to understand the interaction among MPs, CG and XG, we analyzed the variation of particle size. Fig. 1A and B illustrated the particle size and zeta potential characteristics of MPs-CG-XG mixture. Particle size serves as a crucial indicator of the degree of sample aggregation and significantly influences the gelling properties of composite gels. As shown in Fig. 1A, with the increase of XG ratio, the average particle size of MPs-CG-XG mixture gradually increased, from 1234 nm to 2815 nm. This finding was consistent with previous studies, which showed higher formation of protein aggregates in the system (Xu et al., 2021). The addition of CG and XG causes the internal structure of the protein molecule to unfold, which promotes the binding of CG-XG and protein, ultimately leading to the formation of larger polymers (Li

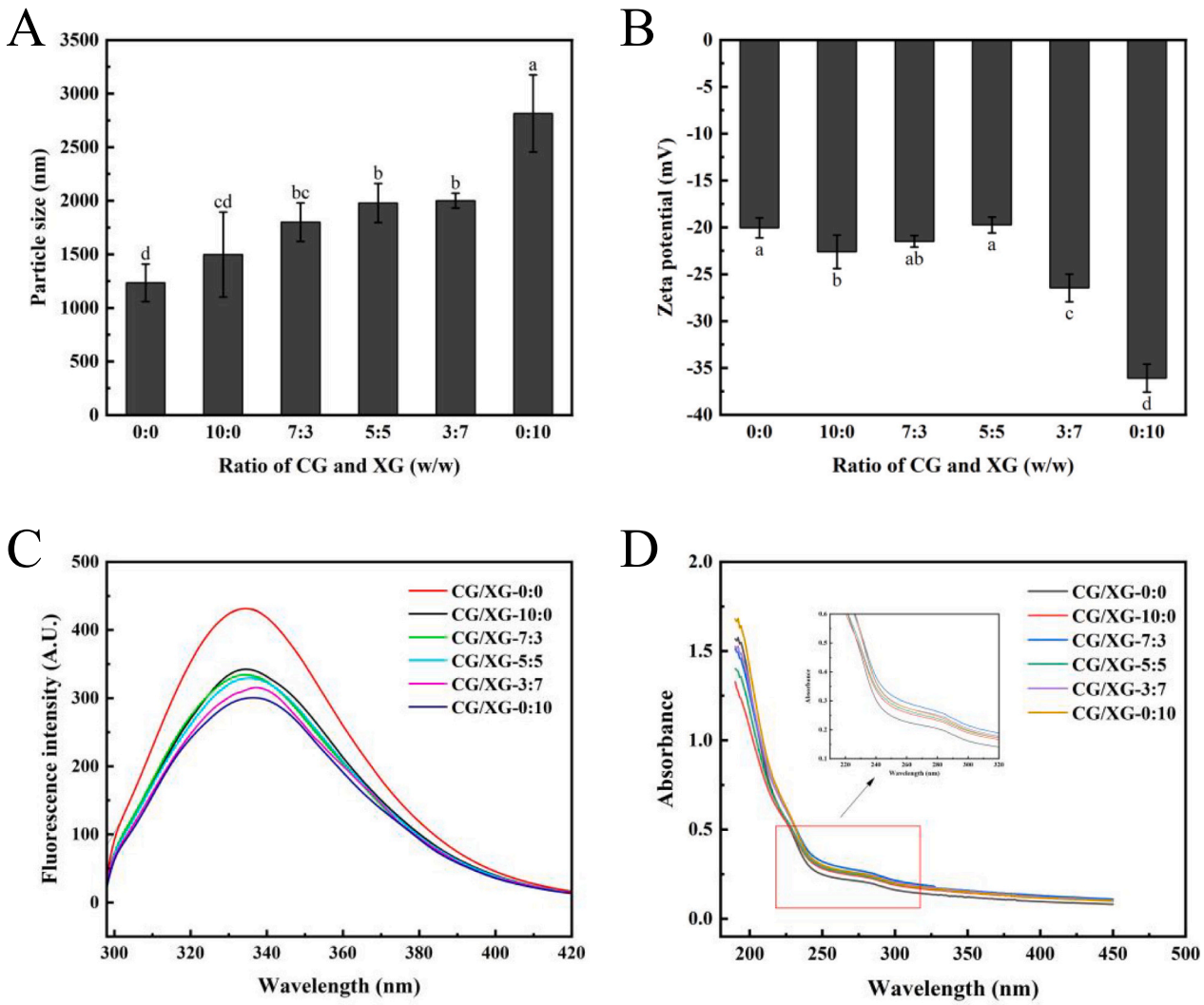

Fig. 1. (A) The particle size of MPs-CG-XG mixtures in different ratios of CG-XG. (B) The zeta potential of MPs-CG-XG mixtures in different ratios of CG-XG. (C) The fluorescence intensity of MPs-CG-XG mixtures in different ratios of CG-XG. (D) The UV–Vis spectrum of MPs-CG-XG mixtures in different ratios of CG-XG. Different letters above the bars indicate significant differences among groups ($P < 0.05$).

et al., 2019). Zeta potential is a key index to characterize the attractive force and repulsive force between macromolecules in aqueous environment, and the higher the absolute value of zeta potential, the more stable the system (Zhang, Li, et al., 2025). As shown in Fig. 1B, the zeta potential of MPs-CG-XG mixture was found to be negative, similar to that of MPs, which may be attributed to the higher content of acidic amino acids. During the mixing process with CG and XG, the proteins undergo expansion, exposing a greater number of acidic groups, thereby contributing to the overall negative charge. Notably, with the addition of CG-XG in varying proportions, the absolute value of the zeta potential exhibited an increasing trend, indicating a rise in surface negative charge density. These changes can be primarily attributed to the interactions between CG-XG and MPs. XG being an anionic polysaccharide, alters the aggregation state and charge distribution of the proteins upon its addition. As shown in Fig. 1B, the absolute value of zeta potential of MPs mixtures increased with the increase of XG addition ratio, indicating that the surface charge density increased. These changes are mainly attributed to the interaction between XG and MPs. The addition of XG will change the aggregation state and charge distribution of protein. It was noteworthy that as the proportion of XG increases, the average particle size of the system also increased, while the absolute value of the Zeta potential exhibited an upward trend. This observation suggested that the addition of XG altered the stability mechanism of the system. The increase in particle size can primarily be attributed to the adsorption of anionic XG chains onto the surface of protein particles, resulting in the formation of larger, loose aggregates that significantly enhance their diameter (Guo et al., 2024). The increase in the absolute value of the Zeta potential was attributable to the adsorption or binding of XG, an anionic polysaccharide, to the surface of MP, which markedly increased the net negative charge density of the complex. Collectively, these two phenomena indicated that at elevated XG concentrations, the stability of the system transitions from being predominantly reliant on electrostatic repulsion to being governed by a synergistic stability mechanism that combined electrostatic repulsion with the substantial spatial steric hindrance provided by the XG adsorption layer.

As illustrated in Fig. 1C, the addition of CG-XG to MPs at specific concentrations and varying proportions resulted in a decrease in fluorescence intensity across all samples. Notably, the fluorescence intensity of the MPs-CG-XG mixture diminished progressively with an increasing ratio of XG. This phenomenon may be attributed to XG's nature as an anionic polysaccharide, which can induce strong interactions with proteins, leading to a reduction in fluorescence intensity (Huang et al., 2022). Furthermore, the fluorescence spectra exhibited a slight red shift corresponding to changes in the CG-XG ratio, likely due to the exposure of hydrophobic groups in MPs-CG-XG mixture system, which leads to the aggregation or charge transfer interaction between MPs and CG-XG. The changes observed in the fluorescence spectra suggested that the addition of CG and XG induced a conformational transition in the MP molecule, leading to the exposure of the hydrophobic core and an increase in the polarity of the surrounding microenvironment. This phenomenon not only enhanced the hydrophobic interactions among protein molecules but also significantly exposed numerous potential hydrogen bond sites and binding sites. Consequently, CG and XG can bind more effectively to the protein molecules, forming stable complexes. During the subsequent thermal gelation process, these pre-formed complexes served as enhanced cross-linking points, which, in conjunction with the protein matrix that aggregated through hydrophobic interactions, contributed to the formation of a more densely cross-linked and structurally uniform composite gel network (Chen et al., 2021).

UV–Vis absorption measurement is a straightforward method for investigating structural changes in proteins and determining whether new complexes are formed between small molecules and proteins. The absorption spectrum of proteins exhibited a peak near 280 nm, which corresponds to aromatic amino acids (Zhang et al., 2020). Fig. 1D illustrated the absorption spectra of MPs with varying proportions of CG-XG added. It was evident that the addition of CG-XG enhanced the absorbance of MPs, and this addition also led to a slight red shift in the position of the maximum absorption peak. These two observations suggested that a new complex is formed through the interaction between CG-XG and MPs.

3.2. Characterization of texture characteristics of MPs-CG-XG gels

In order to testify the gelling properties of MPs influenced by the different ratios of CG and XG, the investigations on texture characteristics of MPs-CG-XG gels formed by heating of MPs-CG-XG mixture were conducted, including several texture parameters of hardness, elasticity, cohesiveness, gel strength, chewiness, and resilience. As shown in Fig. 2A, the initial addition of CG resulted in a decrease in the hardness of the MPs-CG gels compared to the MPs gels. However, the incorporation of XG into the CG-XG system caused the hardness values to first increase and then decrease, with a peak observed at a 5:5 ratio (CG-XG), measuring 99 g higher than that of the MPs gels. Texture, particularly hardness and elasticity, plays a crucial role in determining the palatability and taste of food as it simulates the chewing process. The subjective evaluation of the taste and texture of a gel during chewing typically depends on its hardness and chewiness, which serve as indicators of its mechanical properties. These results suggested that the different proportions of CG and XG in MPs could dramatically influenced the hardness of MPs-CG-XG gels probably in associating the spatial network structure of the gel through hydrogen bonding. The springiness is defined as the ability of an object to return to its original shape upon the removal of a deforming force. Consequently, it is considered one of the most important indices in gel evaluation. As shown in Fig. 2B, the springiness of MPs-CG-XG gels mixed in varying proportions of CG-XG system showed minimal differences among different groups, only revealing the slight descent of springiness values. It was noteworthy that the addition of CG-XG system negatively contributed to the springiness of MPs. Numerous studies have reported that the addition of polysaccharides could enhance both the hardness and springiness of the gel; however, excessively high concentrations may impede the formation of gel networks due to increased system viscosity, ultimately resulting in reduced elasticity (Wang & Hartel, 2022), which could be the reason to explain our results.

Furthermore, other texture property parameters, such as chewiness, resilience, gumminess, and hardness, were also measured, with the results demonstrating similar trends, which was consistent with the hardness results tendency (Fig. 2A). As the concentration of XG in CG-XG system increased, the hardness values of the MPs-CG-XG gels, which facilitated its formation and subsequently enhanced its chewiness, resilience, and gumminess (Fig. 2C, D, and E). Fig. 2F illustrated the effect of different proportions of CG and XG on the cohesiveness of MPs gels sample. The data indicated that as the concentration of XG in the CG-XG system increased, the cohesiveness of the samples initially raised before subsequently declining, When the ratio of CG-XG is 5:5, its cohesion reaches the maximum. Notably, when the CG-XG ratio was 0:10, cohesiveness experienced a resurgence. This phenomenon may be attributed to the varying proportions of CG and XG, which causes different changes in the internal structure of the samples.

According to the experimental results, it was observed that neither CG nor XG alone could enhance the texture of the samples. However, when CG-XG were combined in a 5:5 ratio, all texture parameters improved significantly. This indicated that the mixture of CG-XG at a 5:5 ratio effectively enhanced the texture of MPs. The underlying mechanism may involve the rigid network of CG interpenetrating with the flexible chains of XG, resulting in a ‘rigid-flexible’ composite gel structure that contributes to improved gel strength. Additionally, equal mixing of the two colloids prevented phase separation that could occur due to the high concentration of a single colloid, leading to a more uniform gel. The deterioration of the MPs gels when solely using CG could be attributed to the reliance of the MPs gels on the recombination

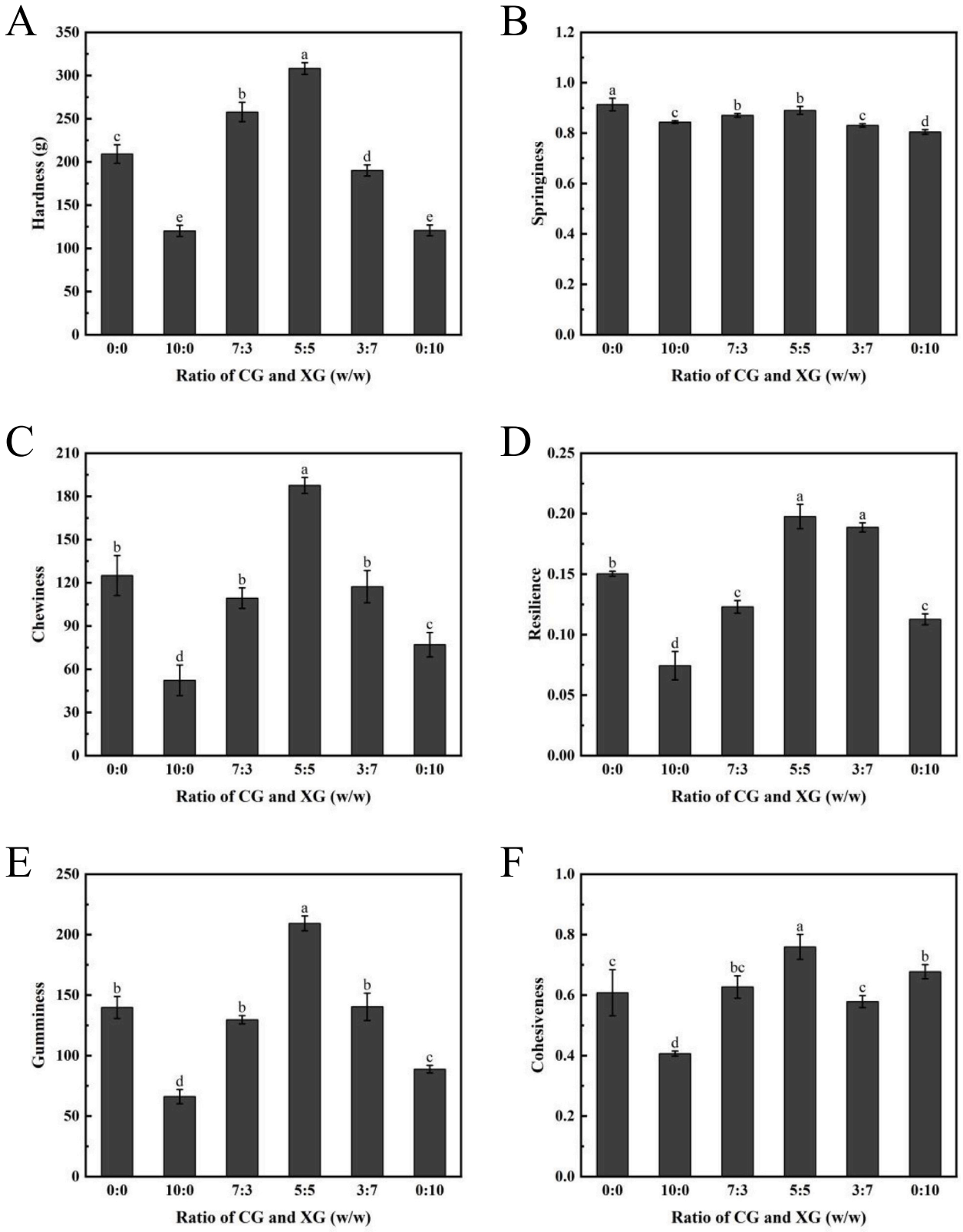

Fig. 2. (A) Hardness of MPs-CG-XG gels with different ratio of CG-XG. (B) Springiness of MPs-CG-XG gels with different ratio of CG-XG. (C) Chewiness of MPs-CG-XG gels with different ratio of CG-XG. (D) Resilience of MPs-CG-XG gels with different ratio of CG-XG. (E) Gumminess of MPs-CG-XG gels with different ratio of CG-XG. (F) Cohesiveness of MPs-CG-XG gels with different ratio of CG-XG. Different letters above the bars indicate significant differences among groups ($P < 0.05$).

of myosin and the formation of disulfide bonds. The robust network formed by CG might physically obstruct the cross-linking between protein molecules, thereby hindering the formation of a continuous and uniform gel structure. Furthermore, the compatibility of CG with MPs is poor, and the separate addition of CG and MPs may lead to a heterogeneous structure, which diminishes the overall uniformity of the gel. The anionic electrostatic repulsion and high viscosity of XG can inhibit the formation of the protein network, resulting in the softening of the MPs gels and a degradation of its texture characteristics.

3.3. Characterization of color characteristics of MPs-CG-XG gels

The color evaluations during food processing are the critical indicator of quality grade. The visual representation of color changes and measurement results of the compound MPs gels, formed by incorporating polysaccharides in varying proportions, was illustrated in Fig. 3A demonstrated that the color of the MPs gels containing CG-XG markedly differed from that of the MPs gels without any gelling agents. The measurement results (Fig. 3B, C, D) indicated that the addition of CG significantly enhances the brightness (L* value). As the concentration of XG in the CG-XG system increased, the brightness gradually decreased, ultimately approaching and slightly falling below that of the MPs gels. The a* value initially decreased before increasing with variations in the CG-XG ratio. Similarly, the b* value also exhibited a decrease followed by an increase in response to changes in the CG-XG ratio, resulting in a gradual deepening of yellow color. These results suggested that CG could enhance the transparency and brightness of the gel whereas the increasement of XG in the CG-XG system dramatically inhibited the gel color, including darkness (decrease in L* value), redness (increase in a* value), and yellowness (increase in b* value), which might be attributed to the inherent yellow natural color of XG. During the heating process of the entire system, full swelling reduced the brightness of the gel; however, the combination of CG and XG in specific proportions can mitigate the impact of xanthan gum on gel color to some extent (Rather et al., 2015). The color of meat products is an important indicator of consumers intuitive perception of quality. Good color can not only enhance the sensory appeal of products, but also imply the suitability of protein stability and antioxidant degree during processing. Therefore, appropriate ratios of CG and XG can be incorporated into meat products to enhance their color.

3.4. Characterization of gel properties of MPs-CG-XG gels

Gel strength is a critical index for assessing the mechanical properties

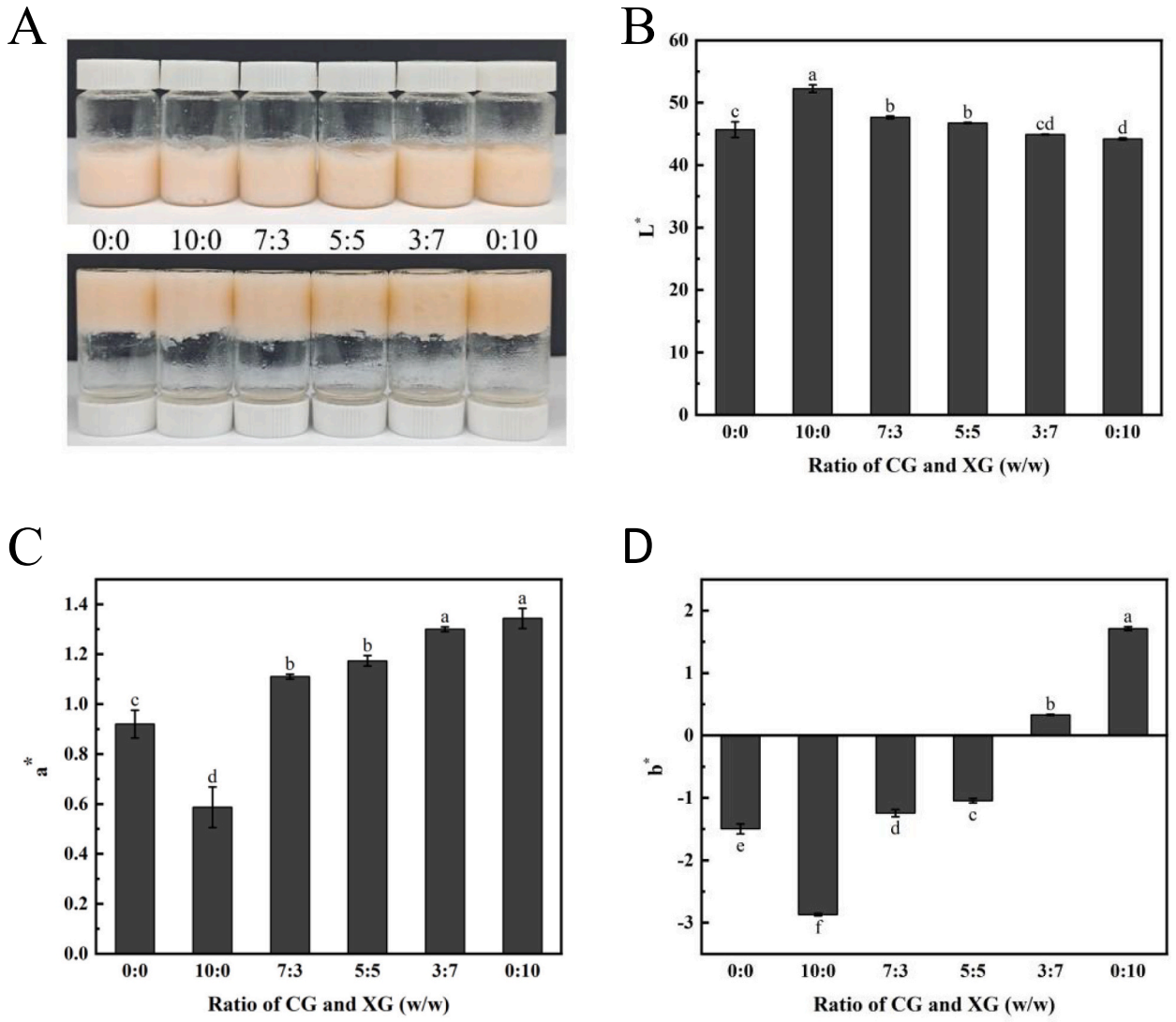

Fig. 3. (A) Images of upright and inverted samples of MPs-CG-XG gels with different ratios of CG-XG. (B) The L* value of MPs-CG-XG gels with different ratios of CG-XG. (C) The a* value of MPs-CG-XG gels with different ratios of CG-XG. (D) The b* value of MPs-CG-XG gels with different ratios of CG-XG. Different letters above the bars indicate significant differences among groups ($P < 0.05$).

of gel materials, reflecting their ability to resist deformation or failure under external forces. As illustrated in Fig. 4A, the results indicated that the gel strength of MPs-CG-XG gels significantly increased with the incorporation of the CG-XG system, suggesting that the addition of CG and XG facilitated the formation of a more uniform and dense network structure within the MPs gels. Notably, when the mass ratio of CG to XG was 5:5, the gel strength values reached their maximum. Meanwhile, gels exhibiting a uniform and dense network structure contribute to enhanced gel strength and water-holding capacity (Li, Yu, et al., 2024). Consequently, as depicted in Fig. 4B, the WHC values of MPs-CG-XG gels at varying mass ratios were evaluated while results indicated that of the MPs-CG-XG gels showed consistent increase in a ratio-dependent manner ($P < 0.05$). This phenomenon could be attributed to several key factors: CG exhibited excellent water absorption and retention, achieving the highest absorption and retention relative to its own containment in water. When incorporated into MPs, the free water within the protein gel would be significantly retained and this network facilitated the incorporation of water molecules into a gel structure through swelling, thereby enhancing the WHC of MPs-CG-XG gels. Consequently, with the introduction of XG, the WHC values of the MPs-CG-XG gels increased progressively until the CG-XG ratio reached 0:10, at which point it attained its maximum value. The results indicated that XG possessed a considerably higher capacity to bind water compared to CG. When the ratio of CG-XG was 3:7, the WHC of the MPs gels achieved the combined effect of MPs and XG, suggesting that the molecular chains of CG and XG were crosslinked (Zhou et al., 2024). The CG-XG mixtures could trap a substantial amount of water within dense gel networks, and the hydroxyl groups in these blends can form hydrogen bonds with the hydrogen atoms in water molecules, thereby enhancing water retention (Du et al., 2021). Overall, these findings indicated that the MPs gels containing CG and XG exhibited superior water retention, with optimal performance observed at mass ratios of 3:7 and 0:10.

The water distribution in MPs-CG-XG gels was also analyzed using LF-NMR. The relaxation times of various MPs-CG-XG gels were illustrated in the Fig. 4C. Typically, the T_2 relaxation time of the gel exhibited four peaks within the range of 0.01 to 1000 ms, with each peak representing a distinct water state. The four identified groups were T_{2b} (0.1–1 ms, representing tightly bound water associated with protein molecules), T_{21} (1–10 ms, indicating partially non-fluidizable water), T_{22} (10–1000 ms, denoting non-fluidizable water), and T_{23} (1000–10,000 ms, corresponding to free water) (Guo et al., 2018). As demonstrated, MPs-CG-XG gels contained these four water states described above. Given that T_{22} comprises the largest proportion of water in the gel system, the relaxation time was utilized to analyze the water distribution state within the MPs-CG-XG gels. Shortening the relaxation time means that the fluidity of water decreases, while lengthening the relaxation time means that the fluidity of water increase (Qin et al., 2015). As shown in Fig. 4C, the addition of CG resulted in a

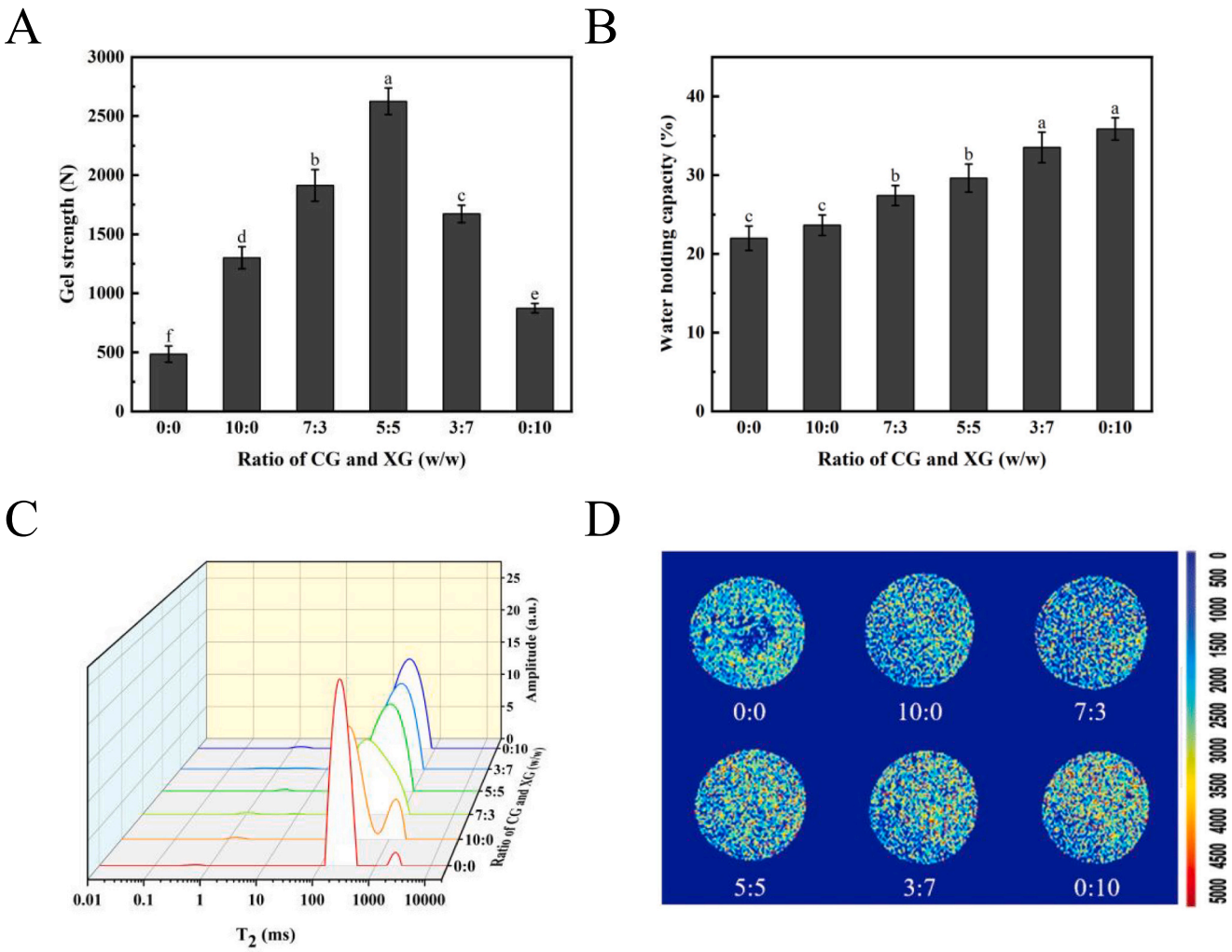

Fig. 4. (A) Gel strength of MPs-CG-XG gels at different CG-XG ratios. (B) WHC of MPs-CG-XG gels with different ratio of CG-XG. (C) T_2 relaxation time profiles of MPs-CG-XG gels at different CG-XG ratios. (D) T_2 weighted magnetic resonance images of MPs-CG-XG gels at different CG-XG ratios. Different letters above the bars indicated significant differences among groups ($P < 0.05$).

decrease in the relaxation time of the MPs gels. Furthermore, the incorporation of XG led to a gradual reduction in relaxation time, suggesting that CG may diminish the fluidity of water within the MPs gels. Notably, the combined effects of CG and XG on reducing the fluidity of water in the MPs gels were more pronounced. The figure further demonstrated that with the incorporation of CG and XG, the peak area corresponding to free water, denoted as T_{23}, significantly diminished, while the collective peak area of low mobile water ($T_{21} + T_{22}$) saw a gradual rise. This finding suggested that free water present in the protein gel converted to low mobile water as heating occurred, thus minimizing moisture loss throughout the cooking process. In this investigation, the observed enhancement in the water retention capacity of the gels, attributed to the varying proportions of polysaccharides added, could be associated with the decrease in T_{22} relaxation time and the simultaneous rise in the peak ratio (Xue et al., 2018). It is noteworthy that the LF-NMR T_2 relaxation data exhibited a distinct optimal ratio trend in comparison to WHC. This discrepancy may arise from the fact that WHC and LF-NMR T_2 relaxation time encapsulated different dimensions of water binding. WHC primarily indicated the network's capacity to resist macroscopic water loss, while LF-NMR relaxation was more adept at revealing the microscopic state and binding strength of water molecules within the gel. The exceedingly high XG content physically obstructed the overall flow and excretion of water in the system by imparting a significantly high macroscopic viscosity, thereby demonstrating remarkable water retention capabilities in centrifugal tests. However, this high-viscosity state may impose restrictions on the microscopic mobility of water molecules, which may not be the most optimal condition. Conversely, at a 5:5 ratio, CG and XG established a dense and uniform interpenetrating network that not only provided minute spaces for physical confinement but also achieved tight chemical hydration of water molecules through robust hydrogen bonding. This dual mechanism of 'chemical-physical' strong binding resulted in minimal (shortest T_2) freedom for water molecule movement. Nevertheless, the network structure may display different dehydration behaviors compared to high-viscosity systems when subjected to extreme centrifugal forces due to its slightly enhanced rigidity.

MRI visualizes the distribution of hydrogen protons through weighted images that reflect proton density within the sample, providing a more intuitive representation of water distribution (Li et al., 2020). As illustrated in Fig. 4D, pseudo-color images of MPs-CG-XG gels with different ratio are presented. Among these samples, the signal intensity of the MPs-CG-XG gels increased with the addition of CG and XG, and the red areas of the pseudo-color images also gradually intensified with changes in the CG-XG ratio. Notably, when the ratio of CG-XG was 3:7 and 0:10, the MPs-CG-XG gels exhibited higher signal intensity, characterized by brighter and redder proton densities. This indicated an increase in the density of hydrogen protons and a more stringent restriction on the movement of water molecules. This observation was consistent with the results depicted in Fig. 4B.

3.5. Determinations of conformational properties of MPs-CG-XG gels

FTIR is utilized to examine the variations in functional groups found in biomacromolecules through peak differences. The structure and flexibility of biopolymers significantly influence their chemical reactivity, intermolecular interactions, and functional characteristics

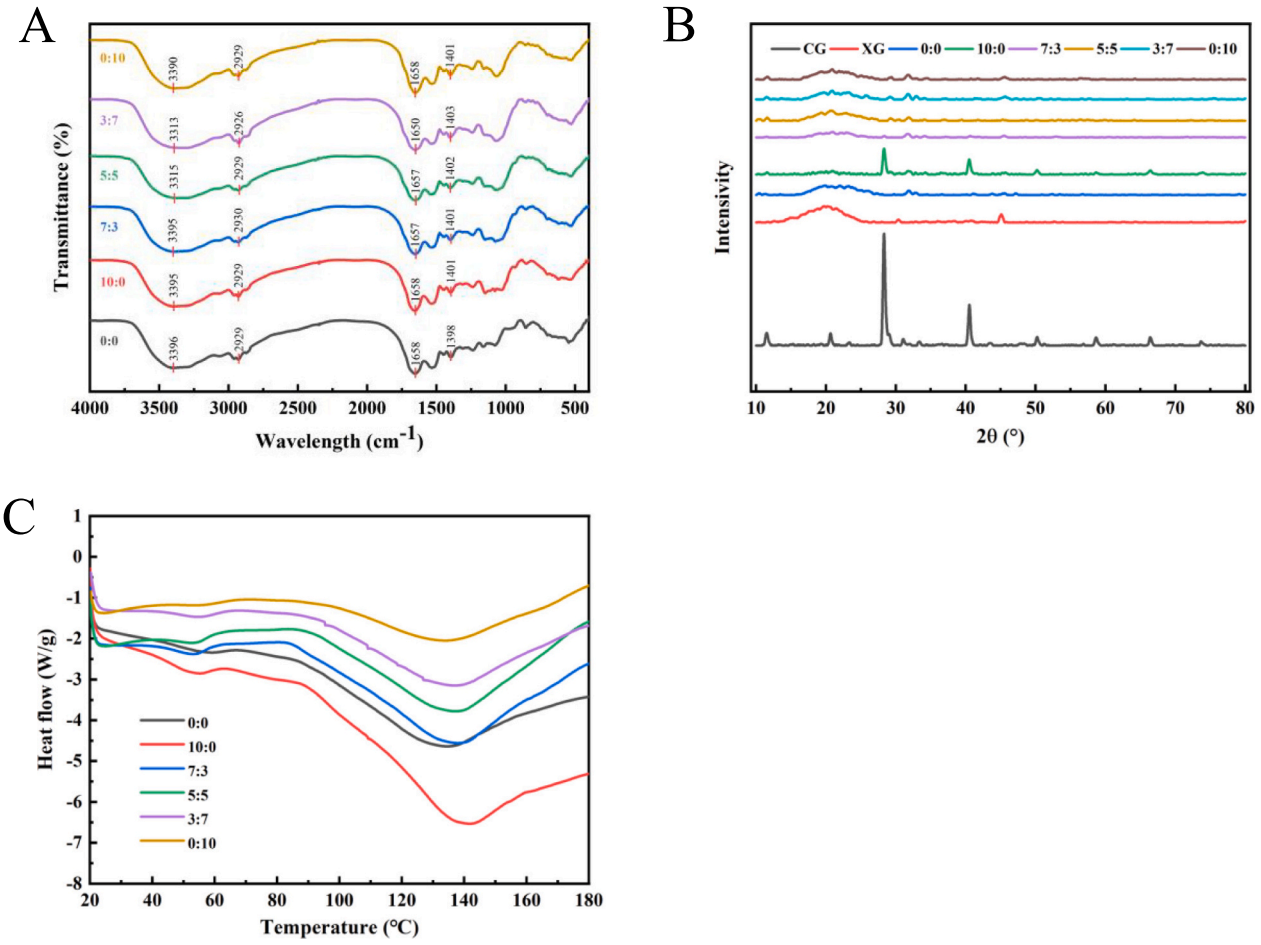

Fig. 5. (A) The FTIR spectra of MPs-CG-XG gels with different ratio of CG-XG. (B) XRD patterns of MPs-CG-XG gels with different ratio of CG-XG. (C) DSC patterns of MPs-CG-XG gels with different ratio of CG-XG.

(Qazvini et al., 2012). Fig. 5A presents the spectra of the MPs-CG-XG gels across different ratios. For MPs, the peaks at 1658 cm^{-1} and 1398 cm^{-1} correspond to the asymmetric and symmetric stretching of the -COO group, respectively. The shoulder observed around 2929 cm^{-1} is linked to C—H stretching in alkanes (Fernandes et al., 2018), while the peak at 3396 cm^{-1} pertains to -OH stretching. When the CG-XG system is combined with MPs, a blue shift occurs in the hydroxyl vibration peak of the resulting complex. Particularly, the blue shifts for MPs-CG-XG gels at

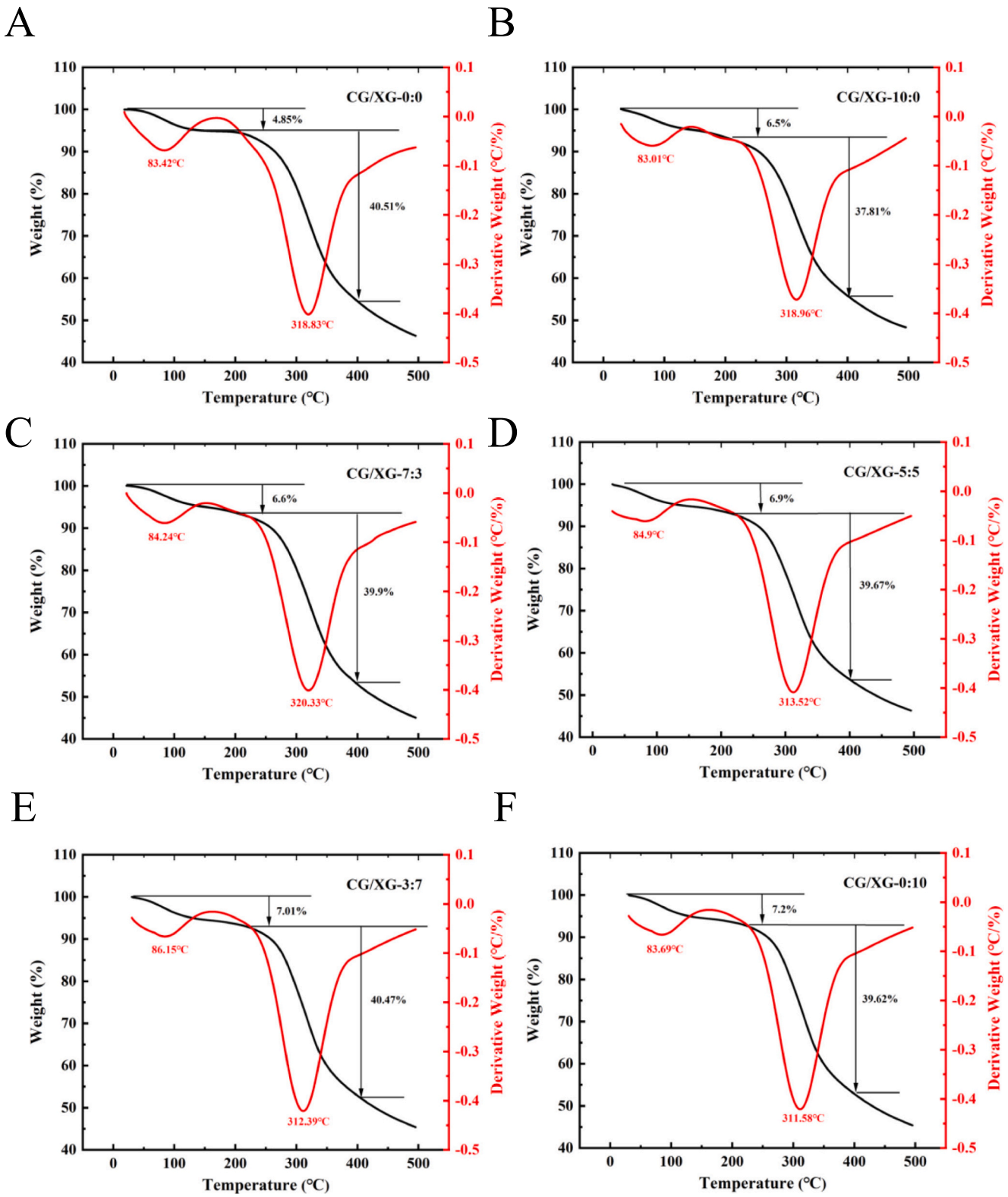

Fig. 6. (A) Thermogravimetric analysis of MP gel. (B) Thermogravimetric analysis of MPs-CG-XG gels at CG-XG = 10:0. (C) Thermogravimetric analysis of MPs-CG-XG gels at CG-XG = 7:3. (D) Thermogravimetric analysis of MPs-CG-XG gels at CG-XG = 5:5. (E) Thermogravimetric analysis of MPs-CG-XG gels at CG-XG = 3:7. (F) Thermogravimetric analysis of MPs-CG-XG gels at CG-XG = 0:10.

ratios of 5:5 and 3:7, recorded at 3315 cm^{-1} and 3313 cm^{-1}, respectively, were more notable than those for MPs-CG or MPs-XG alone. This shift to a lower wave number may result from the complex vibrational stretching of the -OH group, both between and within the molecules. Such behavior serves as compelling evidence for the establishment of hydrogen bonds in MPs-CG-XG gels. Moreover, with an increase in XG content, the carbonyl stretching vibration peak at 1658 cm^{-1} transitioned to the range of 1650 cm^{-1} to 1657 cm^{-1}, indicating the potential electrostatic interaction. Overall, based on the FTIR analysis, it can be concluded that MP formed a composite gel network with CG and XG mainly through hydrogen bonds and electrostatic interactions. The introduction of CG and XG led to changes in the properties of the MP gel.

The diffraction peaks of MPs and XG exhibit broad crystalline and amorphous characteristics, whereas the characteristic diffraction peaks of CG are observed at approximately 28.3° and 40.5°, indicating that CG possesses a crystalline structure. Upon mixing MPs and CG and subsequently heating to form a gel, the diffraction peaks at 28.3° and 40.5° were weakened. With the continuous addition of XG, the diffraction peaks of the blends weakened more significantly, and the positions and intensities of the remaining diffraction peaks varied. When the ratio of CG-XG was 0:10, the characteristic diffraction peaks of CG vanished, and the positions and intensities of the diffraction peaks of MPs-XG differ from those of XG itself. This indicated that the addition of XG further disrupted the crystalline structure of CG. The disruption of the CG crystal structure resulted in the molecular chains breaking away from their tightly packed crystalline state, which increased their mobility and exposed a greater number of hydrophilic groups. In this state, the molecular chains of CG were fully extended and effectively engaged in intermolecular entanglements and hydrogen bond interactions with the negatively charged XG flexible chains and the denatured MP molecules, as indicated by the FTIR results, rather than merely existing in a separated aggregate form. Consequently, the disruption of the CG crystal structure facilitates the homogeneous mixing and interaction of CG, XG, and MP at the molecular level, thereby establishing a foundation for the formation of a uniform and dense composite gel network (Wu et al., 2023).

The interactions between MPs molecules, as well as between MPs and CG-XG, can be characterized using DSC curves. Fig. 5C illustrated the typical DSC curves for MPs-CG-XG gels. Compared to pure MP gels, the samples containing the addition of CG-XG demonstrated a significant increase in peak temperature, particularly at the ratios of CG:XG of 7:3 and 5:5. This observation suggested that, at these specific ratios, the thermal stability of proteins within the composite gel network had been enhanced. This enhancement was likely due to the synergistic interaction between CG and XG, which formed a stable cross-linked microenvironment around the protein molecules, thereby increasing their resistance to thermal disturbances in their native conformation. This finding reinforced the previously proposed mechanism that CG/XG stabilizes and strengthens the MP gel network through molecular interactions from a thermodynamic perspective.

3.6. Evaluations of thermal stability of MPs-CG-XG gels

The influence of CG-XG on the thermal stability of MPs gel was studied by TG and TG derivatives. TGA represents the residual mass curve for a sample that undergoes decomposition as the temperature rises during heating, while DTG reflects the first derivative of the TGA curve in relation to temperature. As shown in Fig. 6A, gels composed of MPs-CG-XG display distinctive thermal decomposition characteristics, marked by degradation occurring at varying temperatures based on their thermal stability differences. The MPs-CG-XG gels exhibited three distinct stages of weight loss during heating (20–500 °C). The initial phase of weight loss occurred at temperatures below 200 °C, accompanied by a mass loss of approximately 6–7%, primarily due to the evaporation of residual water in the gel, which was also associated with the cleavage of intermolecular hydrogen bonds. The mass loss rate at this stage increased with the addition of CG-XG system, meaning the alteration of the hygroscopic properties of the MPs gels caused by CG-XG system. The second phase of weight loss occurred between 200 °C and 400 °C, corresponding to the highest weight loss observed. In MPs-CG-XG gels, this weight loss might be attributed to the disruption of interactions between proteins and polysaccharides, including hydrogen bonds and intermolecular interactions, as well as the breakdown of the network structure of the MPs-CG-XG gel. The control group began to decompose at 318.83 °C, whereas the decomposition temperature of the experimental groups with a CG and CG-XG ratio of 7:3 was higher than that of the control group. Conversely, the decomposition temperature of the experimental groups with a CG-XG ratio of 7:3 was lower than that of the control group. This observation indicates that CG can interact with MPs to enhance the stability of the MPs-CG-XG gels structure, thereby improving the thermal stability of the MPs-CG-XG gels. The addition of XG decreases the thermal stability of the MPs-CG-XG gels, likely due to the strong hydrophilicity of XG, which can bind a significant amount of free water in the system through hydrogen bonds, consequently reducing the hydration layer of MPs. In a dehydrated state, the protein is more prone to expand its conformation due to thermal vibration, which accelerates thermal denaturation. The third degradation phase occurs between 400 °C and 500 °C and corresponds to the complete fragmentation of the protein backbone and disruption of the network structure. This phase is characterized by weight loss and the conversion of the gel to carbon residues due to the degradation of the remaining polysaccharides. The residual mass fraction of MPs was 8.1%, while the residual mass fraction of the gel increased to 8.8% when the ratio of CG-XG was 7:3. This indicates that the weight loss of the MPs-CG-XG gels is lower than that of the MPs gels, suggesting that its thermal stability has improved (Xie et al., 2021). This phenomenon may be attributed to the breakage of MPs and polysaccharide molecular chains; a higher CG content binds to MPs, creating more chemical bonds, therefore, a stronger covalent bond network is formed in MPs-CG-XG gels, thereby increasing the residual content and enhancing thermal stability. These results indicate that the composite gel has thermal stability, which is necessary to maintain its structural integrity in the food industry.

3.7. Determinations of rheology properties of MPs-CG-XG gels

Rheological behavior refers to the viscoelastic changes of gels under external forces. The rheological analysis of MPs and MPs-CG-XG gels, including strain, shear viscosity, and frequency sweep, was presented in Fig. 7A-7D. The storage modulus (G') assesses the material's resistance to elastic deformation, providing insights into its solid elastic characteristics. In contrast, the loss modulus (G") evaluates the resistance to fluid flow, highlighting the sample's viscous properties (Yan et al., 2019). Initially, the linear viscoelastic region (LVE) of the specimen was established via strain sweep testing, where G' and G" displayed rather smooth strain regions, signifying the linear viscoelastic areas of the specimen, the range is from 0.1% to 10% (Fig. 7A). G' > G" was observed for all MPs-CG-XG gels before the strain reaches a critical value, it is shown that the elastic properties of solid are similar to those of solid in this state. To clarify the rheological behavior of the mixed gels, frequency sweep experiments were conducted within the LVE range of 0.1%–10%. As shown in Fig. 7B&7C, The G' values of all MPs-CG-XG gels (10:0, 7:3, 5:5, 3:7, 0:10) exceeded the G" values throughout the frequency range. Furthermore, after CG-XG was added, G' and G" values of MPs-CG-XG gels were gradually higher than MPs gels. When the ratio of CG-XG was 5:5, both G' and G" reached their maximum values. This indicated a strong interaction between CG-XG and MPs, so as to form a stable and compact gel structure and enhance elasticity and viscosity of that gel (Hu et al., 2021). Apparent viscosity versus shear rate curves for MPs gels and MPs-CG-XG gels were shown in Fig. 7D. The observed viscosity of all MPs-CG-XG gels (10:0, 7:3, 5:5, 3:7, 0:10) significantly diminished as the shear rate increased, showcasing a characteristic shear-thinning behavior. Moreover, the addition of CG and XG

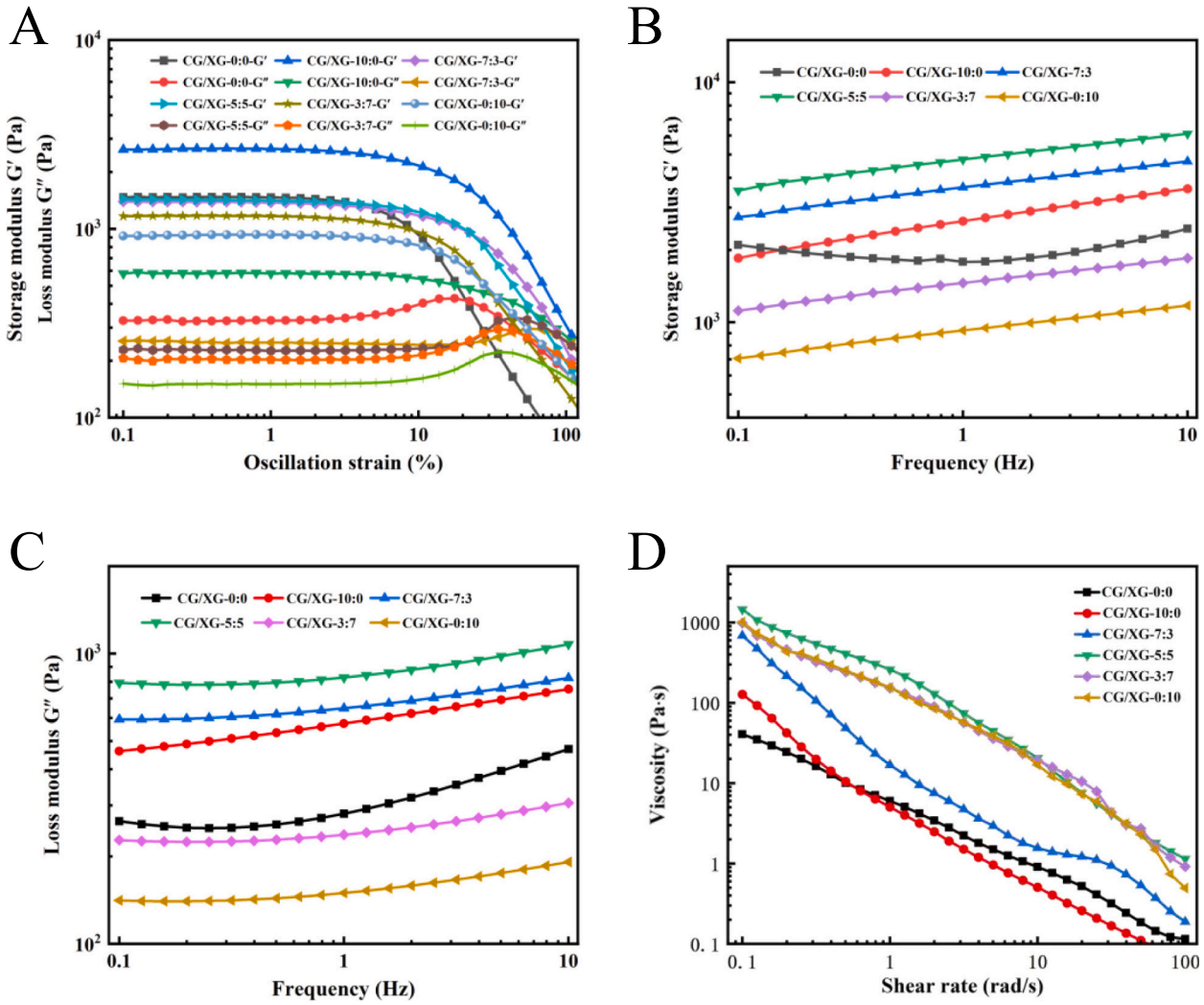

Fig. 7. (A) Storage modulus (G'), loss modulus (G")-oscillation strain profiles of MPs-CG-XG gels with different ratio of CG-XG. (B) Frequency sweep of storage modulus (G') of MPs-CG-XG gels at different CG-XG ratios. (C) Frequency sweep plot of loss modulus (G") of MPs-CG-XG gels at different CG-XG ratios. (D) Viscosity of MPs-CG-XG gels with different ratio of CG-XG.

significantly increased the apparent viscosity of MPs-CG-XG gels, indicating enhanced intermolecular interactions within the gel networks.

3.8. Determinations of morphological appearances of MPs-CG-XG gels

AFM technology is employed to directly characterize the microscopic morphological changes associated with protein aggregation (Yan et al., 2022). Fig. 8A presented the AFM topography of MPs-CG-XG gels with varying proportions of CG-XG system. When CG was added to MPs alone, the aggregated particles observed were small and unevenly distributed, it may be because CG itself has a small particle size, and the polymer formed is large but small and dispersed. In contrast, the addition of an appropriate amount of XG initiated aggregation, resulting in more uniform particle sizes, which indicated that MPs, CG, and XG interact synergistically. At a CG-XG ratio of 5:5, the average size of the aggregates increased, and their distribution became more uniform. However, further increasing the XG (CG-XG ratio of 3:7 or 0:10) content led to enhanced surface roughness and clustering phenomena, suggesting that excessive XG promoted the aggregation of MPs molecules and lead to the formation of larger particles. This may be due to the higher viscosity of XG, which facilitates the coalescence of MPs into larger aggregates. These findings indicated that CG and XG significantly influenced the conformational stability of MPs, aligning with previous particle size results.

Fig. 8B illustrated the changes in SEM morphology of MPs-CG-XG gels with varying proportions of polysaccharides. The MPs gels in the control group, which lacked polysaccharides, exhibited a loose and rough surface with numerous large apertures. Upon the addition of CG-XG system, a significant reduction in the voids on the gel surface was observed, resulting in a smoother texture. When the ratio was adjusted to 5:5, the sample surface became notably smooth, with a compact texture and fewer, filled voids. The CG and XG compounds demonstrated an enhanced ability to bind water, effectively incorporating more free water into the gel structure (Zhao et al., 2019), thereby reducing the pores within the protein network and forming a denser network structure. This observation aligned with previous findings regarding water holding capacity and texture characteristics. When the ratio of CG-XG is 5:5, it becomes 3:7 or 0:10, MPs-CG-XG gels network structure became loose and gradually became lamellar. This may be due to the viscosity of XG is too large to cause MPs-CG-XG gels stick together, so that its network structure weakened.

The cryo-SEM micrographs of MPs-CG-XG gels at different mass ratios are shown in Fig. 8C. Clearly, relatively loose and lamellar gel networks of large and unevenly distributed voids were observed in both the single MP gel and MPs-CG-XG gel at CG-XG ratios of 10:0 and 0:10. In MPs-CG-XG gels, the density and uniformity of the gel network

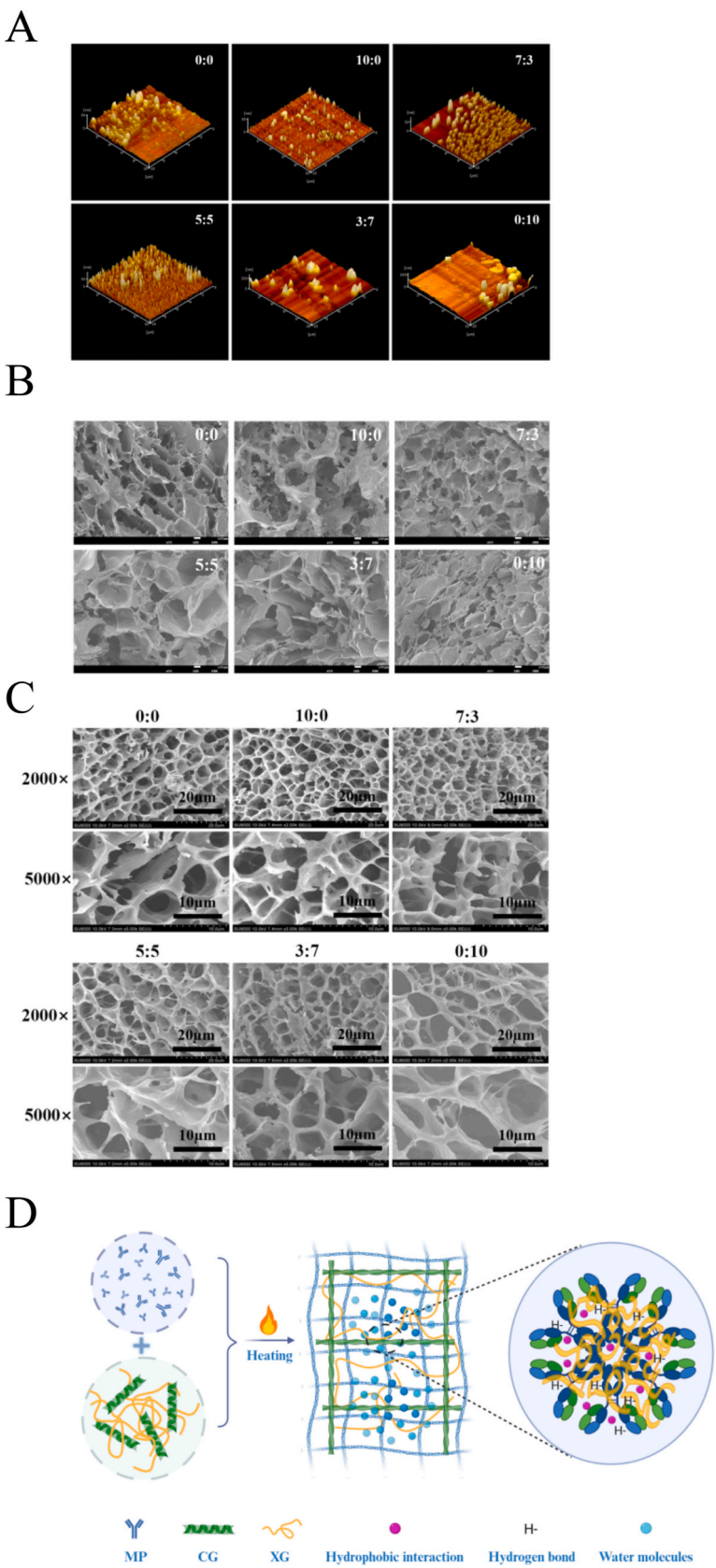

Fig. 8. (A) AFM of MPs-CG-XG mixtures with different proportion of CG-XG. (B) Morphologic appearances of MPs-CG-XG gels with different ratio of CG-XG (SEM images). (C) Cryo-SEM of MPs-CG-XG gels with different ratio of CG-XG. (D) Proposed mechanisms for the formation of MP-CG-XG composite gels.

improved to varying degrees. As the CG-XG ratio increased from 10:0 to 7:3, the gel network became more homogeneous, and the pore sizes decreased, likely due to the synergy between CG and XG. At a CG-XG ratio of 5:5, the MPs-CG-XG gels network exhibited higher density and uniformity compared to other gel networks, with most voids filled. This observation aligned with the rheological data, which indicated that the highest gel strength was achieved at a ratio of 5:5. However, as the CG-XG ratio shifted from 5:5 to 3:7, the gel network began to display microporosity and became heterogeneous and loose, resembling the structure of pure XG and MPs composite gels. When CG-XG ratio is 0:10, the void becomes larger and the surface is smooth. This finding is consistent with the observations of alginate-gellan gum binary composite gels where, with the increase of alginate ratio, the pore size of gel network decreased firstly and then increased obviously, ultimately resembling that of pure alginate gel (Li, Gong, Yang and Guo, 2020). The results showed that MPs -CG-XG gels (CG-XG ratio 5:5) form a denser and more uniform network structure due to intermolecular forces and hydrogen bonds, thus improving the water retention and gel strength of the gels.

Based on the findings, we constructed a mechanism diagram (Fig. 8D) that illustrate the performance enhancement of the MP gel through the incorporation of CG-XG. The rigid framework of CG, the flexible chains of XG, and the denatured MP network collectively form a 'rigid-flexible interpenetrating' composite gel structure via hydrogen bonds, hydrophobic interactions, and physical entanglements. Heating MP at elevated temperatures results in a reduction of hydrogen bonds and an increase in hydrophobic interactions within MP, leading to excessive aggregation of the protein. Consequently, the resultant MP gel contains large protein aggregates and a coarse gel network structure, which diminishes its quality. The addition of CG-XG in equal proportions mitigates the excessive aggregation of MP at high temperatures by reducing the hydrophobic interactions among protein molecules. Simultaneously, it enhances hydrogen bonding, allowing the intermolecular forces between MP molecules to reach equilibrium, thereby forming smaller protein aggregates and a relatively uniform small-pore gel network structure. This modification retains a significant amount of water, thereby improving the quality of the gel network structure to a certain extent.

4. Conclusion

This study demonstrated that when the mass ratio of CG to XG is 5:5, CG and XG exhibited a significant synergistic effect on the gelation of MP. The core mechanism underlying this phenomenon was that the two substances, through intermolecular hydrogen bonding, formed a "rigid-flexible" complementary interpenetrating network structure in conjunction with denatured MP. This network was characterized by a high degree of density and uniformity at the microscopic level, which simultaneously enhanced the mechanical strength, elasticity, and water-binding capacity of the gel at the macroscopic level. It was important to note that the conclusions of this study were based on specific polysaccharide concentrations and ionic strengths under controlled laboratory conditions. The effectiveness of this system in actual complex food matrices required further verification. This work not only elucidated the mechanism by which polysaccharide combinations improved protein gel properties at the molecular interaction level but also provided a clear theoretical basis and formulation framework for developing new shrimp meat gel products with superior texture and high stability. Furthermore, it outlined a direction for future exploration of the application of this composite system in the design of healthy foods and personalized texture regulation.

CRediT authorship contribution statement

Shuling Zhou: Writing – original draft, Investigation, Formal analysis, Data curation. **Xuening Yu:** Data curation. **Menghan Wang:** Data curation. **Xiaoyang Liu:** Writing – review & editing, Supervision, Resources, Funding acquisition, Conceptualization. **Dayong Zhou:** Writing – review & editing.

Declaration of competing interest

The authors declare that they have no known competing financial interests or personal relationships that could have appeared to influence the work reported in this paper.

Acknowledgement

This work was financially supported by the "National Key R&D Program of China (2023YFD2401502)".

Data availability

Data will be made available on request.

References

Chen, B., Guo, J., Xie, Y., Zhou, K., Li, P., & Xu, B. (2021). Modulating the aggregation of myofibrillar protein to alleviate the textural deterioration of protein gels at high temperature: The effect of hydrophobic interactions. *Food Chemistry, 341*, Article 128274.

Du, M., Lu, W., Zhang, Y., Mata, A., & Fang, Y. (2021). Natural polymer-sourced interpenetrating network hydrogels: Fabrication, properties, mechanism and food applications. *Trends in Food Science & Technology, 116*, 342–356.

Feng, J., Bai, X., Li, Y., Kong, B., Nuerjiang, M., Wu, K., Li, Z., & Xia, X. (2023). Improvement on gel properties of myofibrillar protein from chicken patty with potato dietary fiber: Based on the change in myofibrillar protein structure and water state. *International Journal of Biological Macromolecules, 230*, Article 123228.

Fernandes, F. P., Fortes, A. C., da Cruz Fonseca, S. G., Breitkreutz, J., & Ferraz, H. G. (2018). Manufacture and characterization of Mucoadhesive buccal films based on pectin and Gellan gum containing triamcinolone Acetonide. *International Journal of Polymeric Science, 2018*, 1–10.

Ganie, S. A., Rather, L. J., Assiri, M. A., & Li, Q. (2024). Recent innovations (2020−2023) in the approaches for the chemical functionalization of curdlan and pullulan: A mini-review. *International Journal of Biological Macromolecules, 260*, Article 129412.

Gong, H., Liu, J., Wang, L., You, L., Yang, K., Ma, J., & Sun, W. (2022). Strategies to optimize the structural and functional properties of myofibrillar proteins: Physical and biochemical perspectives. *Critical Reviews in Food Science and Nutrition, 64*(13), 4202–4218.

Guo, X., Liu, B., Zhang, Y., Zhou, Y., Gong, Z., Wu, Y., Wang, Q., & Liu, X. (2024). Interfacial structure modification and enhanced emulsification stability of microalgae protein through interaction with anionic polysaccharides. *International Journal of Biological Macromolecules, 283*, Article 137404.

Guo, Y., Hu, H., Wang, Q., & Liu, H. (2018). A novel process for peanut tofu gel: Its texture, microstructure and protein behavioral changes affected by processing conditions. *Lwt, 96*, 140–146.

Hou, X., Liu, X., Zhao, G., Zhang, B., Jiang, F., & Qiao, D. (2024). Self-assembly of curdlan molecules for the formation of thermally induced gels. *Food Hydrocolloids, 156*, Article 110335.

Hu, S., Wu, J., Zhu, B., Du, M., Wu, C., Yu, C., Song, L., & Xu, X. (2021). Low oil emulsion gel stabilized by defatted Antarctic krill (Euphausia superba) protein using high-intensity ultrasound. *Ultrasonics Sonochemistry, 70*, Article 105294.

Huang, X., Sun, L., Liu, L., Wang, G., Luo, P., Tang, D., & Huang, Q. (2022). Study on the mechanism of mulberry polyphenols inhibiting oxidation of beef myofibrillar protein. *Food Chemistry, 372*, Article 131241.

Jiang, Q., Wu, D., Jiang, J., Wu, X., Ma, J., Hu, X., Sun, W., & Liu, J. (2025). Magnetic fields improve the gel properties of myofibrillar proteins in low-salt myofibrillar protein emulsion systems. *Food Chemistry, 470*, Article 142681.

Li, A., Gong, T., Yang, X., & Guo, Y. (2020). Interpenetrating network gels with tunable physical properties: Glucono-δ-lactone induced gelation of mixed Alg/gellan sol systems. *International Journal of Biological Macromolecules, 151*, 257–267.

Li, D., Li, N., Wang, Y., Zhang, K., Tan, Z., Liu, H., Liu, X., Wu, Q., & Zhou, D. (2024). Effect of konjac glucomannan on gelling and digestive properties of myofibrillar protein in Litopenaeus vannamei based on molecular docking. *Food Hydrocolloids, 149*, Article 109595.

Li, D.-Y., Tan, Z.-F., Liu, Z.-Q., Wu, C., Liu, H.-L., Guo, C., & Zhou, D.-Y. (2021). Effect of hydroxyl radical induced oxidation on the physicochemical and gelling properties of shrimp myofibrillar protein and its mechanism. *Food Chemistry, 351*, Article 129344.

Li, G., Yu, X., Xu, Y., Ji, L., Liu, X., Yin, F., Li, D., Xu, B., & Zhou, D. (2024). Recovery effects of sodium carboxymethylcellulose-xanthan gum hydrogels containing peptide-iron complexes against iron deficient anemia in vivo. *International Journal of Biological Macromolecules, 283*, Article 137915.

Li, P., Li, Y., Wang, L., Zhang, H., Qi, X., & Qian, H. (2020). Study on water absorption kinetics of black beans during soaking. *Journal of Food Engineering, 283*, Article 110030.

Li, Z., Wang, J., Zheng, B., & Guo, Z. (2019). Effects of high pressure processing on gelation properties and molecular forces of myosin containing deacetylated konjac glucomannan. *Food Chemistry, 291*, 117–125.
Qazvini, N. T., Bolisetty, S., Adamcik, J., & Mezzenga, R. (2012). Self-healing fish gelatin/sodium montmorillonite biohybrid Coacervates: Structural and rheological characterization. *Biomacromolecules, 13*(7), 2136–2147.
Qin, H., Xu, P., Zhou, C., & Wang, Y. (2015). Effects of l-arginine on water holding capacity and texture of heat-induced gel of salt-soluble proteins from breast muscle. *LWT - Food Science and Technology, 63*(2), 912–918.
Rather, S. A., Masoodi, F. A., Akhter, R., Gani, A., Wani, S. M., & Malik, A. H. (2015). Effects of guar-xanthan gum mixture as fat replacer on the physicochemical properties and oxidative stability of Goshtaba, a traditional Indian meat product. *Journal of Food Processing and Preservation, 39*(6), 2935–2946.
Souza, C. J. F., & Garcia-Rojas, E. E. (2017). Interpolymeric complexing between egg white proteins and xanthan gum: Effect of salt and protein/polysaccharide ratio. *Food Hydrocolloids, 66*, 268–275.
Teng, H., He, Y., Fu, L., Xiong, H., Lu, M., Zhang, C., Ai, C., Cao, H., Zhong, S., & Chen, L. (2023). Effects of blackberry (Rubus spp.) polysaccharide on the structure and thermal behavior of the myofibrillar protein of chicken breast meat. *Food Chemistry, X, 20*, Article 100914.
Wang, J., Shang, M., Li, X., Sang, S., McClements, D. J., Chen, L., … Ji, H. (2023). *Polysaccharide-based colloids as fat replacers in reduced-fat foods. 141* p. 104195).
Wang, R., & Hartel, R. W. (2022). Confectionery gels: Gelling behavior and gel properties of gelatin in concentrated sugar solutions. *Food Hydrocolloids, 124*, Article 107132.
Wu, X., Wang, F., Cai, X., & Wang, S. (2023). Glycosylated peptide-calcium chelate: Characterization, calcium absorption promotion and prebiotic effect. *Food Chemistry, 403*, Article 134335.
Xie, W., Du, Y., Yuan, S., & Pang, J. (2021). Dihydromyricetin incorporated active films based on konjac glucomannan and gellan gum. *International Journal of Biological Macromolecules, 180*, 385–391.
Xu, Y., Yin, Y., Wang, R., Zhao, H., Li, X., Yi, S., Li, J., & Xie, J. (2021). Effect of deacetylated konjac glucomannan on heat-induced structural changes and flavor binding ability of fish myosin. *Food Chemistry, 365*, Article 130540.
Xue, S., Yang, H., Yu, X., Qian, C., Wang, M., Zou, Y., Xu, X., & Zhou, G. (2018). Applications of high pressure to pre-rigor rabbit muscles affect the water characteristics of myosin gels. *Food Chemistry, 240*, 59–66.
Yan, J.-N., Xue, S., Du, Y.-N., Wang, Y.-Q., Xu, S.-Q., & Wu, H.-T. (2022). Influence of pH and blend ratios on the complex coacervation and synergistic enhancement in composite hydrogels from scallop (patinopecten yessoensis) protein hydrolysates and κ-carrageenan/xanthan gum. *Lwt, 154*, Article 112745.
Yan, J.-N., Zhang, M., Zhao, J., Tang, Y., Han, J.-R., Du, Y.-N., Jiang, H., Jin, W.-G., Wu, H.-T., & Zhu, B.-W. (2019). Gel properties of protein hydrolysates from trypsin-treated male gonad of scallop (Patinopecten yessoensis). *Food Hydrocolloids, 90*, 452–461.
Zhang, L., Wang, P., Yang, Z., Du, F., Li, Z., Wu, C., Fang, A., Xu, X., & Zhou, G. (2020). Molecular dynamics simulation exploration of the interaction between curcumin and myosin combined with the results of spectroscopy techniques. *Food Hydrocolloids, 101*, Article 105455.
Zhang, Y., Bai, G., Wang, Y., Wang, J., Teng, W., Li, M., Yao, X., & Cao, J. (2025). Exploring the potential of fibrinogen hydrolysates as enhancers for myofibrillar protein gelation: Insights into molecular assembly behavior. *Food Chemistry, 464*, Article 141587.
Zhang, Y., Li, X., Ge, Y., Hu, Y., Zhu, R., Yang, X., Chen, S., Peng, H., & Wang, C. (2025). Blueberry leaf polysaccharide/gelatin composite gel: Preparation, characterization, and formation mechanism. *International Journal of Biological Macromolecules, 304*, Article 141020.
Zhao, Y., Zhou, G., & Zhang, W. (2019). Effects of regenerated cellulose fiber on the characteristics of myofibrillar protein gels. *Carbohydrate Polymers, 209*, 276–281.
Zhou, T.-Q., Wang, X.-C., Gao, L.-Y., Yan, J.-N., & Wu, H.-T. (2024). Construction and properties of curdlan gum/gellan gum binary composite gel system. *Food Hydrocolloids, 148*, Article 109391.
Zhuang, X., Wang, L., Jiang, X., Chen, Y., & Zhou, G. (2020). The effects of three polysaccharides on the gelation properties of myofibrillar protein: Phase behaviour and moisture stability. *Meat Science, 170*, Article 108228.